Tuning skyrmions in B20 compounds by 4*d* and 5*d* doping

Vladislav Borisov [1,*] Qichen Xu [2,3] Nikolaos Ntallis,[1] Rebecca Clulow [4] Vitalii Shtender [4] Johan Cedervall [5]
Martin Sahlberg [4] Kjartan Thor Wikfeldt [6] Danny Thonig [7,1] Manuel Pereiro [1] Anders Bergman [1]
Anna Delin [2,3] and Olle Eriksson [1,7]

[1]*Department of Physics and Astronomy, Uppsala University, Box 516, SE-75120 Uppsala, Sweden*

[2]*Department of Applied Physics, School of Engineering Sciences, KTH Royal Institute of Technology, AlbaNova University Center, SE-10691 Stockholm, Sweden*

[3]*SeRC (Swedish e-Science Research Center), KTH Royal Institute of Technology, SE-10044 Stockholm, Sweden*

[4]*Department of Chemistry, Uppsala University, Box 538, Uppsala SE-751 21, Sweden*

[5]*Department of Materials and Environmental Chemistry, Stockholm University, SE-10691 Stockholm, Sweden*

[6]*PDC Center for High Performance Computing, KTH Royal Institute of Technology, SE-100 44 Stockholm, Sweden*

[7]*School of Science and Technology, Örebro University, SE-701 82 Örebro, Sweden*

Skyrmion stabilization in novel magnetic systems with the B20 crystal structure is reported here, primarily based on theoretical results. The focus is on the effect of alloying on the 3*d* sublattice of the B20 structure by substitution of heavier 4*d* and 5*d* elements, with the ambition to tune the spin-orbit coupling and its influence on magnetic interactions. State-of-the-art methods based on density functional theory are used to calculate both isotropic and anisotropic exchange interactions. Significant enhancement of the Dzyaloshinskii-Moriya interaction is reported for 5*d*-doped FeSi and CoSi, accompanied by a large modification of the spin stiffness and spiralization. Micromagnetic simulations coupled to atomistic spin-dynamics and *ab initio* magnetic interactions reveal the spin-spiral nature of the magnetic ground state and field-induced skyrmions for all these systems. Especially small skyrmions $\sim$50 nm are predicted for $Co_{0.75}Os_{0.25}Si$, compared to $\sim$148 nm for $Fe_{0.75}Co_{0.25}Si$. Convex-hull analysis suggests that all B20 compounds considered here are structurally stable at elevated temperatures and should be possible to synthesize. This prediction is confirmed experimentally by synthesis and structural analysis of the Ru-doped CoSi systems discussed here, both in powder and in single-crystal forms.

I. INTRODUCTION

Alloy mixtures can sometimes show unexpected properties compared to those of pure components that are used to make up the alloyed state. This is, for example, the case for the Kondo insulator FeSi [1] and the diamagnetic metal CoSi [2], both having the chiral crystal structure of B20 type (Fig. 1). This cubic structure belongs to the $P2_13$ space group, and its chirality becomes apparent when the nearest-neighbor Si atoms for each magnetic transition metal (*TM*) site are considered in terms of the direction of *TM*-Si bonds. While pure FeSi and CoSi do not show any long-range magnetism, an alloyed mixture of them, $Fe_{1-x}Co_xSi$, reveals surprisingly a helical magnetic order in a wide range of concentrations *x* [3,4]. The dependence of these two quantities as well as the helical spatial period on the Co concentration is rather nontrivial,

with the maximal Curie temperature of 50 K and an ordered moment $\sim$0.2 μ_B/f.u. around $x = 40\%$. For a certain range of concentrations, the application of an external magnetic field can induce a skyrmion lattice in these alloys [5,6], similarly to the B20 compound MnSi [7].

The skyrmionic properties of such systems rely on the interplay between the Heisenberg and Dzyaloshinskii-Moriya [8,9] (DM) exchange interactions. The DM interaction (DMI) can actually be significant even if the alloy does not contain heavy elements, which usually contribute to the DMI via their large spin-orbit coupling. Examples of such unexpectedly large DMI are reported in the literature for the oxygen/ferromagnet interface [10] and B20 compounds with 3*d* transition metals [11,12]. For the latter, first-principles calculations [13,14] confirm a significant DM interaction of the order of 1 meV. However, it is natural to expect that the DMI would be further enhanced if the system could contain 4*d* or 5*d* elements, since heavier elements are known to have larger spin-orbit interaction. This idea is corroborated by the experimental observation of robust skyrmions in transition metal multilayers with heavy elements, e.g., Fe/Ir(111) [15], Pt/Co/Ta [16], and Ir/Fe/Co/Pt [17]. Several attempts have been undertaken to synthesize and study the magnetic properties of B20 compounds doped by heavy elements, for example, Rh- and Fe-doped MnGe [18,19] as well as Ir-doped
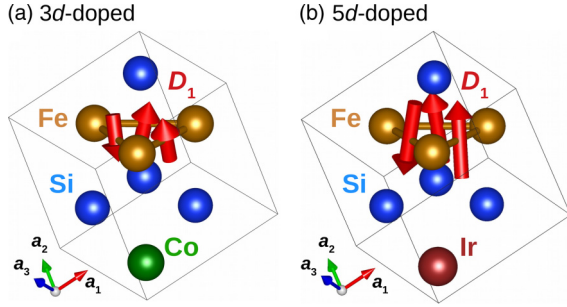
FIG. 1. Dzyaloshinskii-Moriya vectors $(\vec{D}_1)$ for the nearest-neighbor Fe-Fe bonds in the doped B20 compounds: (a) $Fe_{0.75}Co_{0.25}Si$ and (b) $Fe_{0.75}Ir_{0.25}Si$. The direction and size of the DM vectors are given by red arrows, where the arrow length scales with the DMI strength.

MnSi [20] and FeSi [21]. From the study of $Mn_{1-x}Ir_xSi$ [20], it was, however, unclear whether there is any significant change of the DMI with Ir doping, and more accurate ways of extracting the DMI strength from experiment were claimed to be necessary. Concerning $Fe_{1-x}Ir_xSi$ [21], its magnetic properties have been studied experimentally only up to $x = 0.1$, where no long-range order was observed. In general, the effect of $4d$ and $5d$ doping on the magnetic interactions and skyrmions in different B20 compounds has not been systematically explored so far.

In this work, we study theoretically the possibility of improving the skyrmionic properties of FeSi- and CoSi-based B20 compounds by means of $4d$ and $5d$ doping, compared to $3d$ doping. The investigation uses *ab initio* electronic structure theory with a focus on magnetic moments, isotropic Heisenberg exchange, as well as anisotropic interactions (symmetric exchange and DMI). We find a significant enhancement of the calculated DM interaction in FeSi, when 25% Ir is alloyed on the Fe sublattice (Fig. 1), and in Ru- and Os-doped CoSi. This causes the ratio between the DM and Heisenberg interactions to increase substantially, especially for CoSi-based systems. Using these *ab initio* interactions, our simulations of the magnetization dynamics show the spin-spiral nature of the magnetic ground state in zero field and the formation of magnetic skyrmions with topological number 1 when a magnetic field is applied. Convex-hull analysis shows that the considered doped B20 compounds are structurally stable and should be possible to synthesize at elevated temperature, around 1000 K, where the mixing entropy increases the stability. This result is corroborated by a successful synthesis of $Co_{1-x}Ru_xSi$ single crystals that we achieved, which is a class of B20 systems not reported before in the literature.

II. METHODS

The essential aspects of our theoretical simulations are described further below, while all the technical details are discussed in the supporting information (SI) [22].

The structural, electronic, and magnetic properties of doped B20 compounds $Fe_{1-x}TM_xSi$ and $Co_{1-x}TM_xSi$ are studied theoretically using density functional theory (DFT) [23,24] within the generalized-gradient approximation in the PBE parametrization [25]. Previous studies, including our

most recent work [14], suggest that electronic correlations are not crucial for describing the magnetic properties of B20 compounds. Since we are mostly interested in general trends, we do not take into account additional correlation effects beyond the generalized gradient approximation (GGA) in this work.

The doping is simulated within the supercell approach where one of the four Fe or Co magnetic sites in the unit cell is replaced by another $3d$, $4d$, or $5d$ element (Fig. 1), which are Co, Rh, and Ir for FeSi, and Fe, Ru, and Os for CoSi. The supercell structure is optimized using DFT, as available in the VASP code [26], and the calculated structural parameters are summarized in Table I in the SI. Ferromagnetic order is imposed in these and the subsequent DFT calculations. Electronic properties, magnetic moments, and interatomic exchange interactions of the optimized structures are calculated within the all-electron full-potential fully relativistic approach, with linear muffin-tin orbitals as basis functions, as implemented in the RSPt electronic structure code [27–29].

We have calculated magnetic interactions using the relativistic generalization [30–32] of the Lichtenstein-Katsnelson-Antropov-Gubanov (LKAG) formula [33], which we have recently applied to different systems [14]. This involves calculations of all components of the general interaction tensor $\hat{J}$ in the classical Heisenberg model:

$$H = -\sum_{i \neq j} J_{ij}^{\alpha\beta} e_i^{\alpha} e_j^{\beta}, \quad \alpha, \beta = x, y, z, \quad (1)$$

where the unit vectors $\vec{e}_i$ indicate the direction of local spins, and the exchange tensor $J_{ij}^{\alpha\beta}$ contains contributions from the Heisenberg exchange in the diagonal components as well as the DM interaction $\vec{D}$ and the symmetric anisotropic exchange $\hat{\Gamma}$ in the off-diagonal components:

$$\hat{J}_{ij} = \begin{pmatrix} J_{ij} & \Gamma_{ij}^{xy} + D_{ij}^z & \Gamma_{ij}^{xz} - D_{ij}^y \\ \Gamma_{ij}^{xy} - D_{ij}^z & J_{ij} & \Gamma_{ij}^{yz} + D_{ij}^x \\ \Gamma_{ij}^{xz} + D_{ij}^y & \Gamma_{ij}^{yz} - D_{ij}^x & J_{ij} \end{pmatrix}. \quad (2)$$

While the DM interaction is a subject of intense research, the symmetric anisotropic exchange $\hat{\Gamma}$ is seldom discussed in the literature, even though it can be important for the magnetic properties, as demonstrated in the present work. The calculations presented in this section are consistent with previous work [14] and indicate nonzero values of $\hat{\Gamma}$ for the B20 compounds, suggesting that this type of exchange can play an important role for the magnetic properties.

With the first-principles values of the magnetic interactions, the magnetic state is determined as a function of external magnetic field using micromagnetic simulations as implemented in the multiscale module μ-ASD [34] of the UPPASD code [35,36], where the chosen size of the simulated region is $(500 \times 500 \times 100)$ nm. The micromagnetic energy density functional, derived starting from (1), reads

$$E[\vec{m}] = A(\vec{\nabla}\vec{m})^2 + \Gamma^{\alpha\beta}\vec{\nabla}m_\alpha\vec{\nabla}m_\beta + D\vec{m} \cdot (\vec{\nabla} \times \vec{m}). \quad (3)$$

The effective micromagnetic parameters in this model, namely the spin stiffness A, spiralization D, and symmetric exchange $\Gamma^{\alpha\beta}$ ($\alpha, \beta = x, y, z$), are determined from the $\mu \to 0$ limit of direct sums of the atomistic exchange

parameters defined in Eqs. (1) and (2), using the following expressions:

$$A = \frac{1}{2} \sum_{i \neq j} J_{ij} R_{ij}^2 e^{-\mu R_{ij}}, \quad D = \sum_{i \neq j} (\vec{D}_{ij} \cdot \vec{R}_{ij}) e^{-\mu R_{ij}}, \quad (4)$$

$$\Gamma^{\alpha\beta} = \frac{1}{2} \sum_{i \neq j} \Gamma_{ij}^{\alpha\beta} R_{ij}^2 e^{-\mu R_{ij}}. \quad (5)$$

The contribution of the symmetric anisotropic exchange $\Gamma^{\alpha\beta}$ to (3) and expression (5) are derived by us for this work.

For 25%-doped B20 compounds, all components $\Gamma^{\alpha\beta}$ are the same due to the lattice symmetry and the supercells considered in this work. The exponential factor in (4) and (5) is needed for the convergence of the sums with respect to the real-space cutoff radius for R_{ij} (see Sec. IV of SI for technical details), and it was also discussed for evaluations of the spin-stiffness constant [37].

To estimate the possibility of synthesis of the studied B20 compounds, we performed a structural stability analysis using the convex-hull method (workflow in Fig. S6). First, all the competing phases of the target B20 systems were determined by means of data mining with a data-driven high-throughput framework Python Materials Genomics (PYMATGEN) [38], and only records with Inorganic Crystal Structure Database (ICSD) numbers in the Materials Project (MP) Database are selected. Then, the formation energy ΔU for each competing phase was calculated within DFT using open-source material information infrastructure AiiDA [39] and QUANTUM ESPRESSO (QE) software [40,41] (see Sec. V of SI for further details). The formation energy ΔU is defined as the difference between the total energy of the target compound and the total energy of the stoichiometric combination of its constituent pure elements in their standard ground states, e.g., ferromagnetic bcc Fe and hcp Co, and nonmagnetic Si (diamond structure). Based on the obtained ΔU values (Fig. S8), the convex hull diagram (Fig. S7) is constructed from all competing phases using the phase diagram method from PYMATGEN. We also take into account the mixing entropy contribution ΔS to the free energy within the random-alloy approximation: $\Delta S = -k_B[x \ln(x) + (1 - x) \ln(1 - x)]$, where x is the dopant concentration. Since material synthesis usually takes place at elevated temperatures, we set $T = 1000$ K in our calculations to get an estimate of the characteristic magnitude of ΔS.

III. EXPERIMENTAL SECTION

A. Synthesis

Samples of $Co_{1-x}Ru_xSi$ were synthesized by arc melting of stoichiometric quantities of Co (Goodfellow, purity 99.9%), Ru (Cerac, purity 99.95%), and Si (Goodfellow, purity 99.5%) with a 5 at. % excess of Si. Oxidation was minimized by flushing with Ar gas five times and melting a Ti getter before the sample synthesis. The samples were flipped and remelted three times to ensure good homogeneity. The sample was sealed under vacuum in a tantalum tube before annealing at 1773 K for 1 h, slow cooling at 0.1 K/min to 1473 K, and subsequently to room temperature. Single crystals were grown from the as-cast samples, which were crushed and heated in an induction furnace at 1673 K using the Bridgman method.

B. Composition and structure analysis

Powder x-ray diffraction data were measured on a Bruker D8 x-ray diffractometer equipped with a lynx-eye position sensitive detector using Cu $K\alpha$ radiation ($\lambda = 1.5418$ Å). The sample was placed on a zero background single-crystal silicon sample holder during data collection, and the diffraction pattern was collected between $10°$ and $100°$ with a step size of $0.01°$. The data were analyzed using Rietveld refinement [42] within the TOPAS6 software suite [43]. Single-crystal x-ray diffraction data were recorded on a Bruker D8 VENTURE diffractometer at 293 K using Mo $K\alpha_1$ radiation ($\lambda = 0.7107$ Å). The data were processed using the APEX III software [44] and subsequently solved and refined using the SHELX package within the WINGX program [45,46]. The composition of the compounds was investigated by scanning electron microscopy (SEM) using a Zeiss Leo 1550 field emission SEM equipped with an AZtec energy-dispersive x-ray detector (EDS). The samples were prepared by grinding with SiC paper and subsequent polishing with SiO_2 and H_2O. Data were collected on at least 10 points using an accelerating voltage of 20 kV.

IV. RESULTS

A. Heisenberg and DM interactions

The effect of $3d$, $4d$, and $5d$ alloying on the magnetic interactions in FeSi- and CoSi-based B20 compounds is considered first. The main result is a significant enhancement of the DM interaction, which is most pronounced for the $5d$ doping (a comparison between Co- and Ir-doped FeSi is illustrated in Fig. 1, where the size of the interactions is represented by the length of the arrows). Below, we elaborate on this result and discuss further aspects of the exchange interactions of doped B20 compounds.

The calculated element-specific magnetic moments, Heisenberg exchange (J), DM interactions (D), and anisotropic symmetric exchange ($\Gamma^{\alpha\beta}$) are shown in Fig. 2 for 25%-doping of Co, Rh, and Ir in FeSi (similarly, Fig. 3 shows doped CoSi). Significant interactions are observed for spins within a short distance not extending much beyond 6 Å. The short-range character of the interactions is somewhat surprising, given the metallic nature of these systems. On the other hand, for some compounds the simplistic picture with only nearest-neighbor interaction would not be sufficient, since a few further neighboring shells show non-negligible interactions. In terms of the magnitude of the Heisenberg exchange, the Co- and Ir-doped cases are similar [Fig. 2(a)], while Rh doping increases the maximal value of the Heisenberg exchange by $\sim$34 % [Fig. 2(a)]. This can be explained by the relatively large Fe moment of the Rh-doped system (0.97 μ_B in Table I in SI), which is larger than the Co- and Ir-doped systems. Note that in our formalism the lengths of the magnetic moments are incorporated in the exchange interaction; see Eq. (1). In contrast, the DM interaction is only slightly affected by Rh doping compared to Co doping, and a significant enhancement of the largest D_{ij} by $\sim$214 % is only achieved in the Ir-doped case [Fig. 2(b)]. The micromagnetic $\frac{D}{A}$ ratio (Table I in SI and the inverse ratio $\frac{A}{D}$ in Fig. 4) characterizes the relative energy scales of the
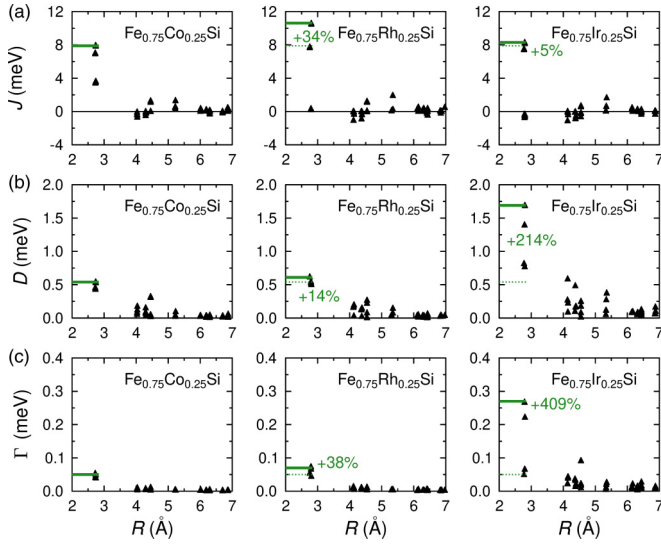
FIG. 2. Evolution of (a) Heisenberg, (b) Dzyaloshinskii-Moriya, and (c) symmetric anisotropic interactions in the doped series $Fe_{0.75}TM_{0.25}Si$ ($TM =$ Co, Rh, Ir). The D and Γ parameters are defined as $D = \sqrt{D_x^2 + D_y^2 + D_z^2}$ and $\Gamma = \sqrt{\Gamma_{xy}^2 + \Gamma_{xz}^2 + \Gamma_{yz}^2}$. The magnetic interactions are calculated for the ferromagnetic reference configuration and are plotted as functions of the distance between the interacting spins. The horizontal green lines mark the maximal value of interaction for each case, and the relative change for the 4d- and 5d-doped cases compared to the 3d-doped case is given in percent.

DM and Heisenberg interactions and is seen to increase in the series 3d-4d-5d, similar to the nearest-neighbor ratio of atomic interactions $\frac{D_1}{J_1}$ (Table I in the SI). Such an enhancement of the DM interaction can lead to skyrmions with smaller geometry.
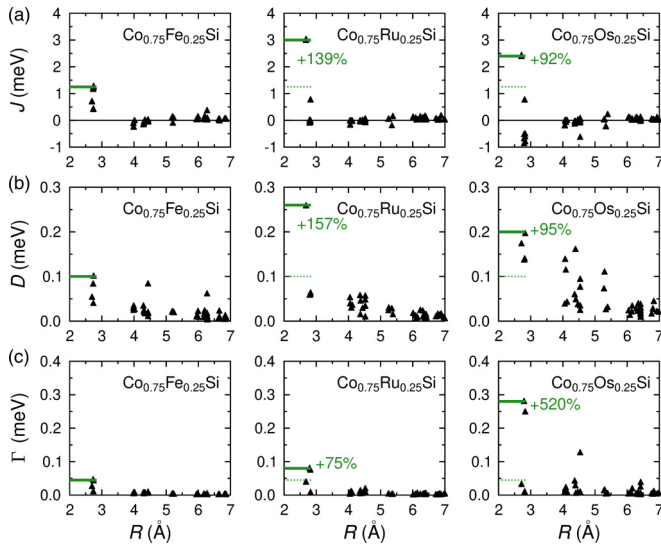

FIG. 3. Evolution of (a) Heisenberg, (b) Dzyaloshinskii-Moriya, and (c) symmetric anisotropic interactions in the doped series $Co_{0.75}TM_{0.25}Si$ ($TM =$ Fe, Ru, Os). The D and Γ parameters are defined as $D = \sqrt{D_x^2 + D_y^2 + D_z^2}$ and $\Gamma = \sqrt{\Gamma_{xy}^2 + \Gamma_{xz}^2 + \Gamma_{yz}^2}$. The magnetic interactions are calculated for the ferromagnetic reference configuration and are plotted as functions of the distance between the interacting spins. The horizontal green lines mark the maximal value of interaction for each case, and the relative change for the 4d- and 5d-doped cases compared to the 3d-doped case is given in percent.
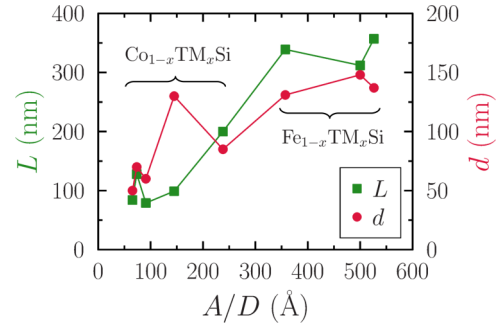

FIG. 4. Relation between the spiral wavelength (left axis, green), skyrmion size (right axis, red), and the $\frac{A}{D}$ ratio for the doped B20 compounds.

Interestingly, the symmetric anisotropic exchange is relatively small in 3d- and 4d-doped FeSi but shows an unexpected increase by 409% for the 5d-doped system [Fig. 2(c)]. However, this exchange interaction is still below 0.3 meV and is not expected to compete with the DM interaction.

In the CoSi-based B20 compounds [Fig. 3(a)], 25%-doping of Fe, Ru, and Os results in a Heisenberg exchange that is a factor of 3 or 4 smaller than in the FeSi-based systems [Fig. 2(a)]. This is related to the significantly weaker magnetic moments of the cobalt-rich systems, as shown in Table I of the SI. We also observe that the Heisenberg exchange J in $Co_{0.75}TM_{0.25}Si$ is much more sensitive to doping than in $Fe_{0.75}TM_{0.25}Si$. Compared to the Fe-doped CoSi, the nearest-neighbor (NN) J-parameter is enhanced by 139% in the Ru-doped CoSi and by 92% in the Os-doped case. Surprisingly, also the DM interaction for some of the NN bonds is increased by up to 157% due to the 4d dopants, while the 5d doping provides an increase of 95% but for several interactions within 5.5 Å [Fig. 3(b)]. It is worth noticing that not only the magnitude but also the direction of the DM vectors is important for noncollinear magnetic textures, and this fact is taken into account in micromagnetic expression (4). The $\frac{D}{A}$ ratio increases considerably for the CoSi systems, reaching 0.015 for the Os-doped case, which, together with the results for FeSi systems, suggests that 5d doping is especially effective for tuning the chiral magnetic interactions in B20 compounds. This conclusion holds for the symmetric anisotropic exchange $\Gamma^{\alpha\beta}$ as well, described by Eq. (5). The magnitude of this symmetric exchange increases by 520% for the Os-doped case compared to the Fe-doped system, remaining, however, below 0.3 meV, similarly to the FeSi systems. The difference is that the DM interactions (D) and symmetric exchange (Γ) are on the same scale for $Co_{0.75}Os_{0.25}Si$ [Figs. 3(b) and 3(c)], which may, in principle, produce interesting magnetic effects. The comparable magnitudes of D and Γ make $Co_{0.75}Os_{0.25}Si$ a unique system, since the symmetric exchange Γ is rarely discussed in the literature, in contrast to the DM interaction. We note that the reason for the predicted increase of the symmetric anisotropic exchange is not clear yet, and although this interaction requires the spin-orbit coupling similarly to the DM interaction, these two types of interactions are not proportional to each other, as can be observed in Table I in the SI.
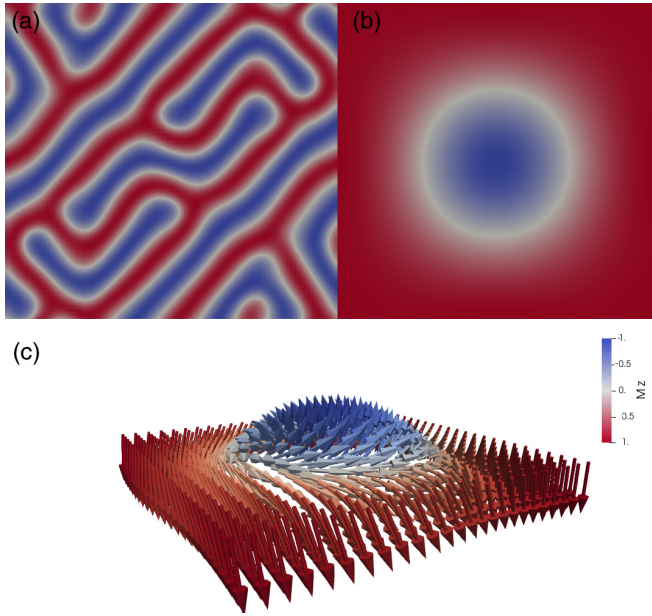
FIG. 5. (a) Helical magnetic state of $Fe_{0.75}Ir_{0.25}Si$, and (b),(c) stabilized skyrmion after the application of magnetic field of 5 mT. (b) Real-space slice of the magnetization showing one skyrmion. (c) The calculated magnetization distribution in the skyrmion shown by arrows. The color indicates the z-component of the magnetic moment, such that the blue (red) color represents the moments pointing fully along the $+z$ direction ($-z$ direction). The total size of the simulation box is (a) $(3 \times 3 \times 1)\,\mu$m and (b) $(0.4 \times 0.4 \times 0.1)\,\mu$m.

The magnetic ordering temperatures were calculated from Monte Carlo simulations and Binder cumulant analysis (see Figs. S1 and S2), and they are summarized in Table I in SI. We see that the ordering temperature T_c is slightly increased by 4d doping both for FeSi and for CoSi compounds, while the 5d doping reduces T_c moderately due to smaller induced moments on 5d atoms and consequently weaker magnetic exchange. While the T_c for CoSi-based systems is around $52 - 56$ K, the critical temperature for FeSi-based systems is overestimated in the DFT calculations, as we discuss in more detail in Sec. 3 of SI. Based on the previous experimental studies of $Fe_{1-x}Co_xSi$, one may expect the actual T_c that would be measured for the studied B20 compounds in the future to be below 30 K. For completeness, we have also calculated the adiabatic magnon spectra of all investigated systems (Fig. S3), following the methodology described in [47], with the most distinct result being a significant magnon band gap around 1.5 meV for $Fe_{0.75}Ir_{0.25}Si$, which may have implications for magnonics.

B. Micromagnetic simulations

Since the wavelength of the spin-spiral ground state of known B20 compounds is of the order of tens or hundreds of nanometers and is too large for atomistic spin dynamics simulations, we have performed micromagnetic simulations with the multiscale module μ-ASD [34] of the UPPASD code [35,36]. The micromagnetic simulation results for the $Fe_{0.75}TM_{0.25}Si$ and $Co_{0.75}TM_{0.25}Si$ compounds in zero magnetic field are depicted in Figs. 5 and S5 in the $(3 \times 3 \times 1)\,\mu$m

region, where the helical domain structure can be appreciated. These results suggest the spin-spiral nature of the magnetic ground state of these B20 compounds. It is apparent that Rh-doped FeSi (Fig. S5b) has the largest spiral wavelength ($L = 357$ nm) while $Fe_{0.75}Co_{0.25}Si$ and $Fe_{0.75}Ir_{0.25}Si$ reveal similar spiral patterns (Table II in SI). We find that the calculated magnetic wavelength L is roughly proportional to the $\frac{A}{D}$ ratio, as illustrated by Fig. 4. We notice that D/A is visibly increased for the Ir-doped FeSi compared to the other two systems (see Table I in SI), indicating a stronger relative contribution of the DM interaction to the magnetic properties. For doped CoSi, the lengthscale of the calculated helical states in Fig. S5 is substantially shorter, which is a consequence of larger D/A ratios. Interestingly, the trends shown by the micromagnetic $|D/A|$ and nearest-neighbor atomistic D_1/J_1 ratios are different, which indicates that an accurate picture of magnetic phenomena must take into account not just the nearest but also further neighbor shells and the direction of the DM vectors that affects $\vec{D}_{ij} \cdot \vec{R}_{ij}$ in Eq. (4).

As an example of a usual procedure to stabilize skyrmions in chiral materials, we show in Fig. 5 the skyrmion state found in $Fe_{0.75}Ir_{0.25}Si$ after the application of an external field of 5 mT. The system does not show the formation of a skyrmion lattice but rather of individual Bloch-type skyrmions, which could be, in principle, manipulated by means of spin currents. The diameter of the stabilized skyrmions is around 131 nm, while the smallest skyrmions are predicted for $Co_{0.75}Os_{0.25}Si$. As expected, we find an increasing linear trend of the skyrmion size as a function of the $\frac{A}{D}$ ratio (Fig. 4). The skyrmion number is 1 for all compounds studied in this work, and, interestingly, the formation of skyrmions in the Co-based B20 systems requires higher magnetic fields compared to FeSi-doped compounds.

C. Phase stability and structural stability from theory

So far, we have discussed the magnetic properties of doped B20 compounds predicted by DFT calculations combined with effective spin Hamiltonians and magnetization dynamics. Since most of these systems have not been studied experimentally yet, it is important to estimate their structural stability, which would indicate whether it is possible to synthesize these doped systems. The previously studied $Fe_{1-x}Co_xSi$ system, which is known from experiments to be stable for $0 \leqslant x \leqslant 1$ [4], can be a reference for validating the chosen theoretical approach and to assess its accuracy.

For all studied B20 compounds, we obtain a negative formation energy around -0.5 eV/f.u. (Fig. S8), which indicates a stability with respect to the decomposition into the pure elements. This condition is necessary but not sufficient, since it does not exclude the decomposition into more complex competing phases, for example, FeSi, CoSi, Fe_3Si, $CoSi_2$, etc., in the case of $Fe_{1-x}Co_xSi$ (further phases are in Fig. S7e). A large number of possible decomposition scenarios can be systematically taken into account by means of a convex hull analysis, the results of which we present in Figs. 6 and S7.

In Fig. S7, the corners of the triangles correspond to the pure constituent elements. Any point inside the triangle is characterized by the projections onto the triangle edges, which indicate the amount of each element in the compound. The
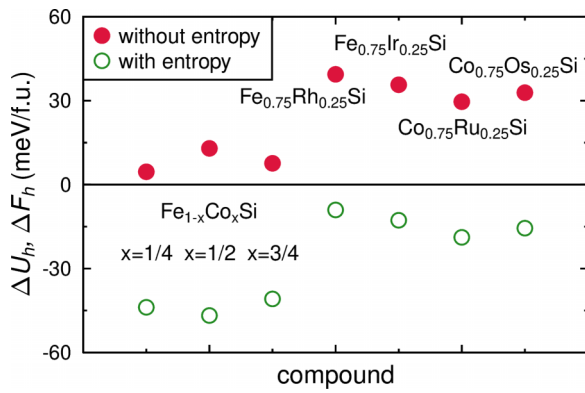
FIG. 6. Distance from the convex hull for doped B20 compounds (from left to right): $Fe_{1-x}Co_xSi$ ($x = \frac{1}{4}, \frac{1}{2}, \frac{3}{4}$), $Fe_{0.75}Rh_{0.25}Si$, $Fe_{0.75}Ir_{0.25}Si$, $Co_{0.75}Ru_{0.25}Si$, and $Co_{0.75}Os_{0.25}Si$. Filled and open symbols correspond to zero-temperature distance ΔU_h (without entropy) and finite-temperature ΔF_h (with mixing entropy, $T = 1000$ K). $\Delta F_h < 0$ indicates a phase and structural stability.

associated formation energy ΔU or free energy ΔF are either above or below the convex hull. The distance from the hull (ΔU_h or ΔF_h) is the main parameter which allows us to judge how stable a particular compound is. Our results summarized in Fig. 6 suggest that ΔF_h are negative for the $Fe_{1-x}Co_xSi$ compounds with $x = \frac{1}{4}$, $\frac{1}{2}$, and $\frac{3}{4}$, which are known to be stable. Since these systems are known to exist, this part of the calculation serves to validate the chosen approach for studying phase and structural stability. It should be noted that $\Delta U_h > 0$ suggests an instability of the system under study. However, the mixing entropy contribution, ΔS, leads to a negative ΔF_h at the chosen temperature, $T = 1000$ K, implying that high-temperature synthesis should be possible. This is indeed the case, as we elaborate in the next paragraph. The mixing entropy, in general, improves the stability of doped systems where a random distribution of impurities is assumed, because ΔS is always positive. Similarly, the $4d$- and $5d$-doped systems are expected to be stable ($\Delta F_h < 0$; see Fig. 6) when the mixing entropy contribution at $T = 1000$ K is taken into account.

D. Synthesis and structure analysis

A series of samples with composition $Co_{1-x}Ru_xSi$ and $x = 0.25$, 0.5, and 0.75 was synthesized by arc melting and analyzed by x-ray diffraction. The powder x-ray diffraction patterns (Figs. S12–S14) confirm that the new compositions adopt the cubic B20 structure type ($P2_13$ space group). The diffraction patterns did not show any evidence of a secondary phase in $Co_{0.75}Ru_{0.25}Si$ and $Co_{0.5}Ru_{0.5}Si$ samples, while the $Co_{0.25}Ru_{0.75}Si$ contained around 2 wt. % of Ru_2Si_3 as previously reported in undoped RuSi [48]. Crystal structure refinement from the powder x-ray diffraction (PXRD) data resulted in unit cell parameters $a = 4.5270$ (1), 4.5919 (1), and 4.6528 (1) Å for compositions with $x = 0.25$, 0.5, and 0.75, respectively. The unit cell parameter increases linearly with Ru content, see Fig. S15, indicating the inclusion of Ru into the crystal structure, and the refined occupancies of the Co/Ru sites were 0.8/0.2, 0.6/0.4, and 0.3/0.7, respectively.

The atomic coordinates and occupancies are given in full in Tables IV, V, and VI in SI and the Rietveld refinement plots in Figs. S12–S14. The composition of the sample was also investigated using energy-dispersive x-ray spectroscopy (EDS) analysis giving values within 2 at. % of the nominal composition (Table IX in SI). Small regions of a secondary phase were observed in the $Co_{0.25}Ru_{0.75}Si$ sample, which corresponded to the Ru_2Si_3 present in the x-ray diffraction pattern. The structure type and space group of $Co_{0.75}Ru_{0.25}Si$ were also confirmed by the single-crystal x-ray diffraction data, the refined unit cell parameter was slightly larger than from PXRD, $a = 4.5629(6)$ Å, and it coincides with a slightly higher refined Ru content of 0.39. The full crystallographic data and refinement details are shown in Tables VII and VIII in SI.

V. CONCLUSION

Using state-of-the-art theoretical methods, we have studied the magnetic interactions and topological textures in $3d$-, $4d$-, and $5d$-doped B20 compounds based on FeSi and CoSi. The most significant finding is that $5d$ doping (by Ir or Os) enhances the Dzyaloshinskii-Moriya interaction considerably, especially for the CoSi systems where the smallest skyrmions around 50 nm are predicted for $Co_{0.75}Os_{0.25}Si$. Interestingly, CoSi-based compounds require a larger magnetic field for skyrmion formation, and in general they show smaller skyrmions compared to the FeSi systems. The magnetic ordering temperature is found to be sensitive to doping, in agreement with the literature, and it is expected to be below 30 K. Based on the convex-hull analysis, we predict that all the studied B20 compounds are structurally stable and can be synthesized at high temperature. For $Co_{1-x}Ru_xSi$ with $x = \frac{1}{4}, \frac{1}{2}, \frac{3}{4}$, we actually report a successful synthesis and characterization.

Our work predicts that $4d$- and $5d$-doped B20 compounds are promising as systems holding skyrmions, with varying size of the skyrmions depending on the system. Our results suggest that $Co_{0.50}Ru_{0.50}Si$ is optimal in terms of the magnetization, $\frac{D}{A}$ ratio, and skyrmion diameter compared to other studied systems. Experimental synthesis shows that several of these compounds can be formed, in particular the $Co_{1-x}Ru_xSi$ system with up to 75% Ru concentration. The results reported here hence demonstrate several new compounds in the family of materials crystallizing in the B20 structure. Theory suggests that several of these are magnetic and can hold magnetic structures with nontrivial topology.

[1] Z. Schlesinger, Z. Fisk, H.-T. Zhang, and M. B. Maple, Phys. B Condensed Matter **237-238**, 460 (1997).

[2] J. H. Wernick, G. K. Wertheim, and R. C. Sherwood, Mater. Res. Bull. **7**, 1431 (1972).

[3] N. Manyala, Y. Sidis, J. F. DiTusa, G. Aeppli, D. Young, and Z. Fisk, Nature (London) **404**, 581 (2000).

[4] Y. Onose, N. Takeshita, C. Terakura, H. Takagi, and Y. Tokura, Phys. Rev. B **72**, 224431 (2005).

[5] W. Münzer, A. Neubauer, T. Adams, S. Mühlbauer, C. Franz, F. Jonietz, R. Georgii, P. Böni, B. Pedersen, M. Schmidt, A. Rosch, and C. Pfleiderer, Phys. Rev. B **81**, 041203(R) (2010).

[6] X. Z. Yu, Y. Onose, N. Kanazawa, J. H. Park, J. H. Han, Y. Matsui, N. Nagaosa, and Y. Tokura, Nature (London) **465**, 901 (2010).

[7] S. Mühlbauer, B. Binz, F. Jonietz, C. Pfleiderer, A. Rosch, A. Neubauer, R. Georgii, and P. Böni, Science **323**, 915 (2009).

[8] I. Dzyaloshinsky, J. Phys. Chem. Solids **4**, 241 (1958).

[9] T. Moriya, Phys. Rev. **120**, 91 (1960).

[10] G. Chen, A. Mascaraque, H. Jia, B. Zimmermann, M. Robertson, R. L. Conte, M. Hoffmann, M. A. G. Barrio, H. Ding, R. Wiesendanger, E. G. Michel, S. Blügel, A. K. Schmid, and K. Liu, Sci. Adv. **6**, eaba4924 (2020).

[11] S.-A. Siegfried, E. V. Altynbaev, N. M. Chubova, V. Dyadkin, D. Chernyshov, E. V. Moskvin, D. Menzel, A. Heinemann, A. Schreyer, and S. V. Grigoriev, Phys. Rev. B **91**, 184406 (2015).

[12] K. V. Shanavas and S. Satpathy, Phys. Rev. B **93**, 195101 (2016).

[13] S. Grytsiuk, M. Hoffmann, J.-P. Hanke, P. Mavropoulos, Y. Mokrousov, G. Bihlmayer, and S. Blügel, Phys. Rev. B **100**, 214406 (2019).

[14] V. Borisov, Y. O. Kvashnin, N. Ntallis, D. Thonig, P. Thunström, M. Pereiro, A. Bergman, E. Sjöqvist, A. Delin, L. Nordström, and O. Eriksson, Phys. Rev. B **103**, 174422 (2021).

[15] S. Heinze, K. v. Bergmann, M. Menzel, J. Brede, A. Kubetzka, R. Wiesendanger, G. Bihlmayer, and S. Blügel, Nat. Phys. **7**, 713 (2011).

[16] L. Wang, C. Liu, N. Mehmood, G. Han, Y. Wang, X. Xu, C. Feng, Z. Hou, Y. Peng, X. Gao, and G. Yu, ACS Appl. Mater. Interfaces **11**, 12098 (2019).

[17] A. Soumyanarayanan, M. Raju, A. L. G. Oyarce, A. K. C. Tan, M.-Y. Im, A. P. Petrović, P. Ho, K. H. Khoo, M. Tran, C. K. Gan, F. Ernult, and C. Panagopoulos, Nat. Mater. **16**, 898 (2017).

[18] S. V. Grigoriev, N. M. Potapova, S.-A. Siegfried, V. A. Dyadkin, E. V. Moskvin, V. Dmitriev, D. Menzel, C. D. Dewhurst, D. Chernyshov, R. A. Sadykov, L. N. Fomicheva, and A. V. Tsvyashchenko, Phys. Rev. Lett. **110**, 207201 (2013).

[19] V. A. Sidorov, A. E. Petrova, N. M. Chtchelkatchev, M. V. Magnitskaya, L. N. Fomicheva, D. A. Salamatin, A. V. Nikolaev, I. P. Zibrov, F. Wilhelm, A. Rogalev, and A. V. Tsvyashchenko, Phys. Rev. B **98**, 125121 (2018).

[20] C. Dhital, L. DeBeer-Schmitt, Q. Zhang, W. Xie, D. P. Young, and J. F. DiTusa, Phys. Rev. B **96**, 214425 (2017).

[21] B. C. Sales, E. C. Jones, B. C. Chakoumakos, J. A. Fernandez-Baca, H. E. Harmon, J. W. Sharp, and E. H. Volckmann, Phys. Rev. B **50**, 8207 (1994).

[22] See Supplemental Material at http://link.aps.org/supplemental/10.1103/PhysRevMaterials.6.084401 for further details about the theoretical and experimental methods and results.

[23] P. Hohenberg and W. Kohn, Phys. Rev. **136**, B864 (1964).

[24] W. Kohn and L. J. Sham, Phys. Rev. **140**, A1133 (1965).

[25] J. P. Perdew, K. Burke, and M. Ernzerhof, Phys. Rev. Lett. **77**, 3865 (1996).

[26] G. Kresse and J. Furthmüller, Phys. Rev. B **54**, 11169 (1996).

[27] J. M. Wills and B. R. Cooper, Phys. Rev. B **36**, 3809 (1987).

[28] J. M. Wills, O. Eriksson, M. Alouani, and D. L. Price, Full-potential LMTO total energy and force calculations, in *Electronic Structure and Physical Properties of Solids*, edited by H. Dreyssé (Springer-Verlag, Berlin, Heidelberg, 2000), doi: 10.1007/3-540-46437-9_4.

[29] J. Wills, M. Alouani, P. Andersson, A. Delin, O. Eriksson, and O. Grechnyev, *Full-Potential Electronic Structure Method* (Springer-Verlag, Berlin, Heidelberg, 2010), Vol. 167, doi: 10.1007/978-3-642-15144-6.

[30] L. Udvardi, L. Szunyogh, K. Palotás, and P. Weinberger, Phys. Rev. B **68**, 104436 (2003).

[31] H. Ebert and S. Mankovsky, Phys. Rev. B **79**, 045209 (2009).

[32] Y. O. Kvashnin, A. Bergman, A. I. Lichtenstein, and M. I. Katsnelson, Phys. Rev. B **102**, 115162 (2020).

[33] A. Liechtenstein, M. Katsnelson, V. Antropov, and V. Gubanov, J. Magn. Magn. Mater. **67**, 65 (1987).

[34] E. Mendez, M. Poluektov, G. Kreiss, O. Eriksson, and M. Pereiro, Phys. Rev. Research **2**, 013092 (2020).

[35] B. Skubic, J. Hellsvik, L. Nordström, and O. Eriksson, J. Phys.: Condens. Matter **20**, 315203 (2008).

[36] O. Eriksson, A. Bergman, L. Bergqvist, and J. Hellsvik, *Atomistic Spin Dynamics: Foundations and Applications* (Oxford University Press, Oxford, UK, 2017), https://global.oup.com/academic/product/atomistic-spin-dynamics-9780198788669?cc=us&lang=en&.

[37] M. Pajda, J. Kudrnovský, I. Turek, V. Drchal, and P. Bruno, Phys. Rev. B **64**, 174402 (2001).

[38] S. P. Ong, W. D. Richards, A. Jain, G. Hautier, M. Kocher, S. Cholia, D. Gunter, V. L. Chevrier, K. A. Persson, and G. Ceder, Comput. Mater. Sci. **68**, 314 (2013).

[39] S. P. Huber, S. Zoupanos, M. Uhrin, L. Talirz, L. Kahle, R. Häuselmann, D. Gresch, T. Müller, A. V. Yakutovich, C. W. Andersen *et al.*, Sci. Data **7**, 300 (2020).

[40] P. Giannozzi, S. Baroni, N. Bonini, M. Calandra, R. Car, C. Cavazzoni, D. Ceresoli, G. L. Chiarotti, M. Cococcioni, I. Dabo *et al.*, J. Phys.: Condens. Matter **21**, 395502 (2009).

[41] P. Giannozzi, O. Andreussi, T. Brumme, O. Bunau, M. B. Nardelli, M. Calandra, R. Car, C. Cavazzoni, D. Ceresoli, M. Cococcioni *et al.*, J. Phys.: Condens. Matter **29**, 465901 (2017).

[42] H. M. Rietveld, J. Appl. Crystallogr. **2**, 65 (1969).

[43] A. A. Coelho, J. Appl. Crystallogr **51**, 210 (2018).

[44] Bruker AXS Inc., Bruker APEXIII, Madison, WI (2012).

[45] G. M. Sheldrick, Acta Crystallogr. Sect. C **71**, 3 (2015).

[46] L. J. Farrugia, J. Appl. Crystallogr. **45**, 849 (2012).

[47] R. Yadav, M. Pereiro, N. A. Bogdanov, S. Nishimoto, A. Bergman, O. Eriksson, J. van den Brink, and L. Hozoi, Phys. Rev. Materials **2**, 074408 (2018).

[48] L. Perring, F. Bussy, J. Gachon, and P. Feschotte, J. Alloys Compd. **284**, 198 (1999).

[49] K. Momma and F. Izumi, J. Appl. Crystallogr. **44**, 1272 (2011).